RSC Advances

Cite this: *RSC Advances*, 2012, **2**, 2047–2054

www.rsc.org/advances

PAPER

Remarkable fluorescence enhancement in $YVO_4:Eu^{3+}$@Ag nano-hybrids induced by interface effect

Wen Xu, Xue Bai,* Sai Xu, Yongsheng Zhu, Lei Xia and Hongwei Song*

Received 15th September 2011, Accepted 24th November 2011
DOI: 10.1039/c2ra00736c

The luminescence enhancement effect induced by the coupling of noble metal nanoparticles (NPs) with rare earth (RE) doped nanophosphors is attracting current interests. In order to obtain efficient luminescence enhancement and clarify its physical nature, the $YVO_4:Eu^{3+}$@Ag core-shell nano-hybrids colloids were first prepared by a facile two-step seed-mediated growth method. The luminescence enhancement of $^5D_0$–^7F_J transition for Eu^{3+} with a maximal factor of ~one order was observed, which strongly depended on the amount of silver NPs, the concentration of the $YVO_4:Eu^{3+}$ colloids and the dissolved solutions. The enhancement mechanism was carefully discussed based on absorption spectra, emission spectra, luminescent decay dynamics and zeta potentials of colloids solutions. The results indicate that the silver NPs on the surface of $YVO_4:Eu^{3+}$ can effectively prevent VO_4^{3-} and Eu^{3+} from the interaction with the solvent such as OH bonds, leading to a decrease of nonradiative energy transfer (ET) and suppressed luminescent quenching. A detailed model was proposed to explain the interesting luminescence enhancement behavior.

I. Introduction

Rare earth (RE) ions doped nanophosphors (NPs) are attracting extensive current attentions due to their potential applications in lasers,[1] lighting and displays,[2] photon converters for solar cells,[3] biological fluorescence imaging and detections,[4] *etc.* In contrast to the other phosphor species such as organic dyes and semiconductor quantum dots, RE doped NPs demonstrate unique photoluminescent properties, such as plentiful and narrow emission lines, long decay time constants, large stokes shift, quantum cutting and upconversion luminescence and so on.[5–9] In addition, RE doped oxide and fluoride NPs demonstrate high chemical stability, high biocompatibility and low toxicity. These excellent properties make RE doped NPs an important representation in bio-applications.

Although there has been much work in the field, it is still a challenge to effectively improve the brightness and luminescent quantum efficiency of RE doped NPs due to structure defects and their large surface areas with a variety of quenchers which have been formed in the previous preparation process.[10,11] The brightness of RE doped NPs needs to be largely improved for further application, especially for the colloids. A well-known way to enhance the fluorescence of RE doped NPs is the coupling of emitters to metallic surfaces or particles.[12] In the vicinity of metal structures, the electric field distribution is altered and as a result, the excitation field and the emitted radiation can be enhanced. Recently, a number of works have been performed to improve the photoluminescence of RE doped NPs through the coupling of RE ions to noble metallic surfaces or particles[13,14] (silver and gold) in colloids, glasses, or thin films.[12,15] Perriat and co-workers reported the luminescence enhancement of $Gd_2O_3:Tb^{3+}$ NPs attached on gold nanorods (NRs) in a colloidal solution of diethylene glycol and observed a 37-fold enhancement factor,[16] the mechanism was attributed to the resonant energy transfer (ET) between the gold NRs and the RE NPs. Note that in most of literatures, the resonant ET leads to fluorescence quenching of emitters.[17] Some authors observed highly plasmon-enhanced UC emissions from $NaYF_4:Yb^{3+}$, Er^{3+} (Tm^{3+}) @Au or $NaYF_4:Yb^{3+}$, Er^{3+} @Ag colloids and obtained enhancement factors of several fold up to ~two orders.[12a,15f,15g,18] In the literature, two main mechanisms for fluorescence enhancement have been proposed. One mechanism is the surface plasmon induced absorption enhancement of emitters due to the enhancement of the local electric field at the metal nanostructure surface. Another mechanism is the increase in the radiative decay rate of emitters due to the resonance of the emission with the surface plasmon of noble metals. It should be pointed out that in most of literatures, there was a lack of creditable evidence for the origin of fluorescence enhancement. For instance, no one practically observed the absorption enhancement of RE emitters, even in those highly luminescence-enhanced systems. Some authors observed improved decay rate of RE emitters, and others observed a suppressed decay rate.

We believe that in colloids, the RE doped NPs are not only affected by the field enhancement effect, but also influenced by

State Key Laboratory on Integrated Optoelectronics, College of Electronic Science and Engineering, Jilin University, 2699 Qianjin Street, Changchun, 130012, China. E-mail: hwsong2005@yahoo.com.cn; xuebai07@yahoo.com.cn; Fax: +86-431-85155129

an interface effect in the presence of silver or gold nanoparticles/nanoshells. In this work, $YVO_4:Eu^{3+}$ NPs colloids were prepared, which had strong absorption in the UV region and high photoluminescent efficiency in the red region.[19] To obtain enhanced fluorescence, $YVO_4:Eu^{3+}$ @ Ag nano-hybrids colloids were prepared.[20] In the hybrid colloids, it is exciting to observe an enhancement of an order of magnitude higher than the original. In addition, the interaction mechanism between emitters and the silver was systemically studied, which showed that the interface effect, solvent effect and concentration effect were of key importance for the luminescence enhancement of $YVO_4:Eu^{3+}$ @ Ag nano-hybrid colloids.

II. Experimental section

A. Synthesis of $YVO_4:Eu^{3+}$ spheres and $YVO_4:Eu^{3+}$ @ Ag Hybrids

The $YVO_4:Eu^{3+}$ spheres (~150 nm) were prepared *via* the solvothermal method using DMF as the solvent, as according to our previous literature.[21] In a typical synthesis, 0.25 g of $Y(NO_3)_3{\cdot}5H_2O$, 0.01 g of $Eu(NO_3)_3{\cdot}5H_2O$ were first dissolved in DMF (10 ml), then a given amount of CTAB and PVP were added with stirring for one hour, and then 1 ml 2 mol l^{-1} HCl aqueous solution and 0.22 g of $Na_3VO_4{\cdot}12H_2O$ were subsequently added with stirring for another 12 h until the solution became homogenous. After that, the mixture was sealed in a Teflon-lined stainless steel autoclave and heated at 150 °C for 24 h under static conditions and then cooled naturally. $YVO_4:Eu^{3+}$ precipitates were collected and washed three times with alcohol, then air-dried at 60 °C for 24 h. All of the above-mentioned actions were performed under ambient atmosphere.

The coating process was finished by the facile seed-mediated growth procedure,[20] which was simply divided into two steps, seed attachment and seed growth, as shown in the Scheme 1. In the first step, the $YVO_4:Eu^{3+}$ powders (0.04 g) were dispersed in ethanol (10 ml). The suspension was added to the mixed solvents (12 ml, ethanol/acetone volume ratio = 2 : 1) which was saturated with a certain amount of $AgNO_3$ under magnetic stirring at room temperature for one hour. Then the colloids were washed with ethanol by centrifugation to remove excess silver ions, and dispersed in ethanol (20 ml) again. Subsequently, $NaBH_4$ aqueous solution (0.1 M, 1 ml) was added. After one hour, the colloids were once more washed with ethanol to remove excess $NaBH_4$ and dispersed in ethanol (40 ml) for standby. In the second step, a certain amount of standby colloid was added to aqueous and ethanol mixing solvents (volume ratio = 1 : 1) containing sodium nitrate (0.1 M), and different amount of silver nitrate. After that, the same amount of ammonia solution and L-ascorbic acid solution (0.1 M, 1 ml) was added. Finally, the composite colloids were centrifuged and dispersed in ethanol (5 ml) and the mass concentration was about 1 mg ml^{-1}. The corresponding nano-hybrid powders were obtained by air-drying at 60 °C for 24 h.

B. Characterization

The surface morphology of the as-prepared products was recorded on a Hitachi H-8100 IV transmission electron microscope (TEM) under an acceleration voltage of 200 kV. The phase structure and purity of the as-prepared samples were characterized by X-ray power diffraction (XRD) with a Rigaku D/max 2550 X-ray diffractometer, using a monochromatized Cu target radiation resource (λ = 1.54 Å). The absorption spectra were measured with a UV-1800 UV-visible spectrometer. The excitation and emission spectra were recorded at room temperature using a Fluorescence Spectrophotometer. The luminescent quantum efficiency was measured with a Fluorescence spectrophotometer equipped with a $BaSO_4$ integrated sphere. The luminescent dynamics were investigated by a laser-system consisting of a Nd:YAG pumping laser (1064-nm), the third-order Harmonic-Generator (355-nm) and a tunable optical parameter oscillator (OPO, Continuum Precision II 8000). It was with a pulse duration of 10 ns, repetition frequency of 10 Hz and line width of 4–7 cm^{-1}. The zeta potential was investigated using a GG301-Nicomp 380/Zeta PLAS.

III. Results and discussion

A. Morphology and structure of $YVO_4:Eu^{3+}$ @ Ag Nano-hybrids

First, the morphology of the $YVO_4:Eu^{3+}$ spheres and $YVO_4:Eu^{3+}$ @Ag hybrids coated with different amount of silver NPs were examined by HR-TEM images, as shown in Fig. 1. It can be seen that the YVO_4: Eu^{3+} NPs before coating are smooth, uniform and mono-dispersed spheres, with an average diameter of ~150 nm (see Fig. 1(a)). After first-step coating, the surface of YVO_4: Eu^{3+} becomes rough and irregular, implying the formation of very small Ag NPs on the surface (see Fig. 1(b)). After second-step coating with different amounts of silver nitrate ~5 and 200 μM, many distinguishable silver NPs (~8 nm) adhere to the surface of $YVO_4:Eu^{3+}$ NPs, and the number of silver nanoparticles increases largely with the increase of silver nitrate. This structure is similar to some previous literature,[12a,15g,18,22] on $NaYF_4:Yb^{3+}$, Er^{3+} @Au hybrids.

Fig. 2 shows the XRD patterns of the $YVO_4:Eu^{3+}$ NPs, $YVO_4:Eu^{3+}$@Ag hybrids and the corresponding standard cards,

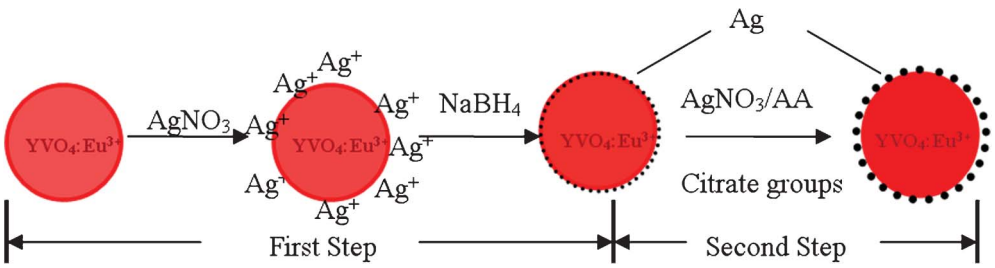

Scheme 1 Schematic illustration of the formation of the $YVO_4:Eu^{3+}$@Ag nano-hybrids.

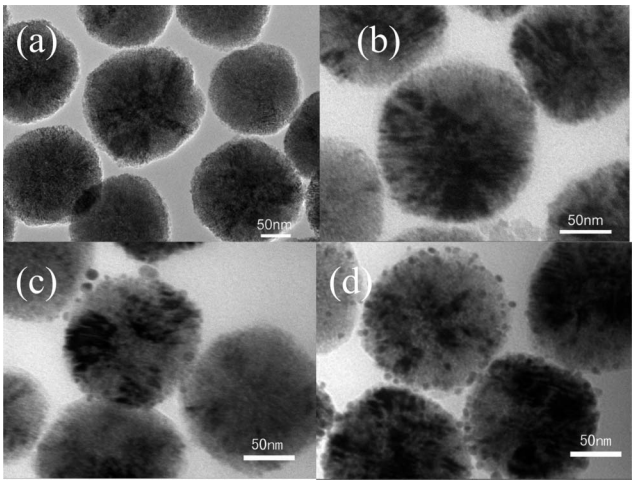

Fig. 1 TEM images of the YVO_4:Eu^{3+} NPs (a) and YVO_4:Eu^{3+}@Ag hybrids prepared with different amount of silver nitrate in second-step deposition (b) 0 μM, (c) 5 μM, and (d) 200 μM.

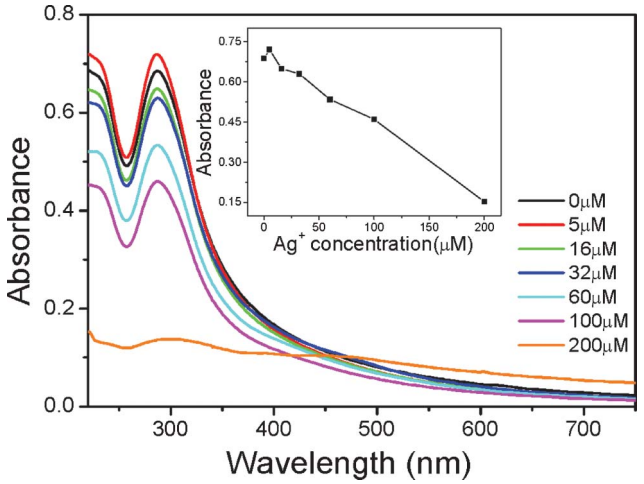

Fig. 3 Absorption spectra of YVO_4:Eu^{3+} NPs and YVO_4:Eu^{3+} @ Ag hybrids with various amounts of silver nitrate.

JCPDS 17-0341 for tetragonal YVO_4 and 87-0717 for cubic silver. It can be seen that the YVO_4:Eu^{3+} sample (curve a) is exactly in agreement with the corresponding standard cards, JCPDS 17-0341 for tetragonal YVO_4. In the YVO_4:Eu^{3+}@Ag hybrids, the *311 face of cubic silver (marked with star) can be clearly distinguished. The *111, *200 and *220 faces for cubic silver overlap with the 202, 103, 204 faces of tetragonal YVO_4, respectively. In the hybrids, the patterns corresponding to *111, *200 and *220 faces relatively increase in contrast to pure YVO_4:Eu^{3+} (see curves b and c), further indicating the formation of YVO_4:Eu^{3+}@Ag hybrids.

Fig. 3 shows the absorption spectra of YVO_4:Eu^{3+} NPs and YVO_4:Eu^{3+}@Ag hybrids with different amounts of silver nitrate dispersed in ethanol solutions (The particle concentration was fixed at 0.07 mg ml^{-1}). A band centering at ~285 nm can be observed for all the solutions, corresponding to the charge transfer absorption from the oxygen to the central vanadium atoms inside the VO_4^{3-}. The band location changes a little with the amount of silver nitrate because of unchanged energy gap between the ground and excited states of VO_4^{3-} spaces.[21] As the amount of silver nitrate increases to 200 μM, another peak appears at 450 nm, which could be assigned to the surface plasmon absorption of silver nanoparticles. The inset of Fig. 3 shows the absorbance at ~285 nm as a function of silver nitrate amount. It can be seen that the absorbance of VO_4^{3-} groups has little variation in the range of 0–16 μM and gradually decreases with the increase of silver nitrate in the range of 32–200 μM. This can be attributed to the scattering and reflection of visible and UV light by silver NPs adhered to the surface of the YVO_4:Eu^{3+} NPs.

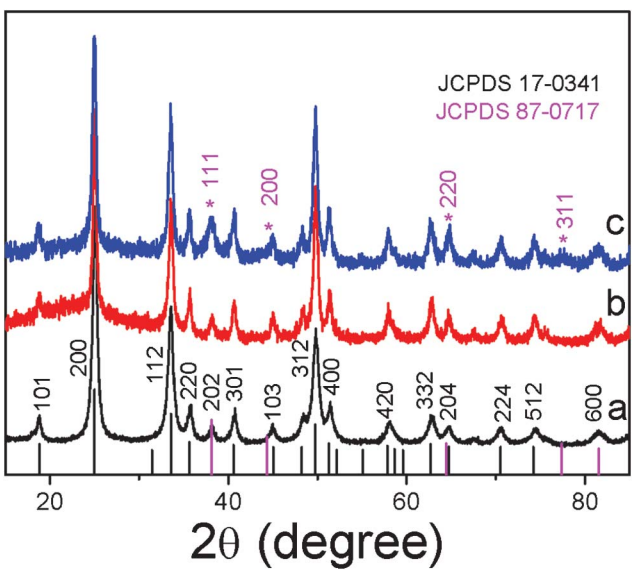

Fig. 2 The XRD patterns of the YVO_4:Eu^{3+} NPs (a) and YVO_4:Eu^{3+}@Ag hybrids prepared with different amount of silver nitrate (b) 5 μM, and (c) 200 μM.

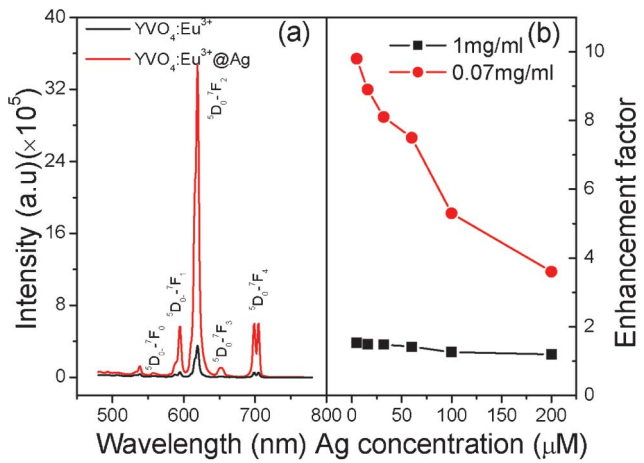

Fig. 4 (a) A comparison of emission spectra between YVO_4:Eu^{3+} NPs and YVO_4:Eu^{3+} @Ag hybrids dispersed in ethanol solution (0.07 mg ml^{-1}). (b) Luminescent enhancement factor as a function of silver nitrate (λ_{ex} = 265 nm).

B. Fluorescence enhancement of $YVO_4:Eu^{3+}$ @ Ag Hybrid Colloids

In $YVO_4:Eu^{3+}$@Ag hybrid colloids, a strong luminescence enhancement was observed—in contrast to the $YVO_4:Eu^{3+}$ NPs—which greatly dependent on the amount of silver NPs on the surface of $YVO_4:Eu^{3+}$ NPs and the concentration of $YVO_4:Eu^{3+}$@Ag in the colloids. Fig. 4(a) shows a comparison of emission spectra between 0.07 mg ml^{-1} of $YVO_4:Eu^{3+}$ NPs and $YVO_4:Eu^{3+}$@Ag (5 μM–$AgNO_3$) hybrids in ethanol solution. The strong red emission of $^5D_0$–^7F_J (J = 0–4) for Eu^{3+} ions was distinguished and labelled in the figure. In contrast to $YVO_4:Eu^{3+}$ NPs, the overall fluorescence intensity of Eu^{3+} in the $YVO_4:Eu^{3+}$@Ag hybrid colloids increases up to 9.8 fold. Fig. 4(b) displays the fluorescence enhancement factor as a function of silver nitrate amount in $YVO_4:Eu^{3+}$@Ag hybrid colloids, which is defined as the ratio of the $^5D_0$–^7F_J emission intensity in $YVO_4:Eu^{3+}$@Ag hybrids to that in the $YVO_4:Eu^{3+}$ NPs. For the 0.07 mg ml^{-1} of $YVO_4:Eu^{3+}$@Ag solution, a 9.8 fold maximum enhancement factor was observed when the amount of silver nitrate was ~5 μM. When the amount of silver nitrate increased continuously from 5 to 200 μM, the fluorescence enhancement factor gradually decreased, until it was 3.6 fold. For the 1.00 mg ml^{-1} of $YVO_4:Eu^{3+}$@Ag dense solution, the fluorescence enhancement factor also decreased with the increase in silver nitrate, varying from 1.6 to 1.15 fold. According to the inset of Fig. 3, it is suggested that the fluorescence suppression with the increase of silver nitrate in Fig. 4 is due to the decrease of incident light caused by the scattering and reflection of silver NPs.

The NP concentration in the $YVO_4:Eu^{3+}$ colloids has an obvious effect on the fluorescence intensity of both the $YVO_4:Eu^{3+}$ colloids[23-25] and the $YVO_4:Eu^{3+}$@Ag nano-hybrids. Fig. 5 shows the dependence of the overall fluorescence intensity of Eu^{3+} on the particle concentration of $YVO_4:Eu^{3+}$or $YVO_4:Eu^{3+}$@ Ag colloids (5 μM silver nitrate). It is interesting to observe that the fluorescence intensity increases with the increasing particle concentration at first (0.01–0.07 mg ml^{-1}) and approaches a maximum at 0.07 mg ml^{-1}, before decreasing when

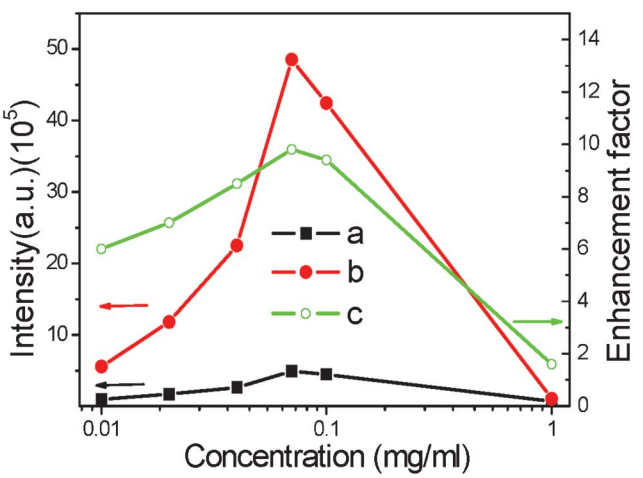

Fig. 5 Dependence of luminescent intensity of $^5D_0$–Σ^7F_J of $YVO_4:Eu^{3+}$ (a) and $YVO_4:Eu^{3+}$ @ Ag hybrids (b) and the enhancement factor (c) on the particle concentration of $YVO_4:Eu^{3+}$ colloids (λ_{ex} = 265 nm).

Table 1 A list of luminescent enhancement (En-) factor of $YVO_4:Eu^{3+}$@Ag (En-factor), the decay lifetime constants of $YVO_4:Eu^{3+}$ NPs (τ_0) and $YVO_4:Eu^{3+}$@Ag (τ_1) in various solvents (The concentration was fixed at 0.01 mg ml^{-1}) and powder samples

Solvent	EG	DMF	H_2O	Ethanol	Powders
En-factor	2.9	1.9	4.0	6.0	1.0 (no)
τ_0(μs)	57	84	92	85	114
τ_1(μs)	138	153	226	141	93

the particle concentration exceeds 0.07 mg ml^{-1} for both the $YVO_4:Eu^{3+}$ NPs and the $YVO_4:Eu^{3+}$@Ag composites. This behavior indicates that if the concentration of NPs is too high, fluorescence quenching will be induced due to the interaction among different NPs.[23] Despite this, the intensity of Eu^{3+} in the $YVO_4:Eu^{3+}$@Ag hybrids is significantly higher than for the $YVO_4:Eu^{3+}$ NPs. Similarly, the fluorescence enhancement factor is related to the particle concentration. It first increases from 6.0 to 9.8 when the concentration ranges between 0.01–0.07 mg ml^{-1}, and approaches a maximum at 0.07 mg ml^{-1}, then decreases from 9.8 to 1.6 as the concentration ranges between 0.07–1.00 mg ml^{-1}.

The luminescent enhancement of $YVO_4:Eu^{3+}$@Ag colloids also strongly depends on the dissolved solutions. Table 1 lists the variation of luminescence enhancement factor with different solutions. It can be observed that as 0.01 mg ml^{-1} of the $YVO_4:Eu^{3+}$@Ag hybrids were dissolved in different solutions, DMF, EG, H_2O and Ethanol, the emission intensity of Eu^{3+} increases 1.9, 2.9, 4.0 and 6.0 fold, in contrast to the corresponding $YVO_4:Eu^{3+}$ solutions. However, the intensity of Eu^{3+} in $YVO_4:Eu^{3+}$@Ag powders keeps nearly constant in comparison to the corresponding $YVO_4:Eu^{3+}$ powders. These results definitely suggest that the luminescence enhancement is induced by the interface effect between the solutions and the NPs, rather than the field enhancement effect, which will be discussed carefully in the next section. It is believed that the species, structure, polarity and optical properties of both solutions have strong influence on the luminescence enhancement of RE-doped NPs, which is a complex proposition to investigate.

C. Improved decay time constants in the $YVO_4:Eu^{3+}$ @ Ag Nano-hybrids

The luminescent decay dynamics of the $^5D_0$–$^7F_2$ transition for $YVO_4:Eu^{3+}$@Ag nano-hybrids as well as $YVO_4:Eu^{3+}$ NPs were also studied. The results demonstrate that all the decay curves can be well fitted by a biexponential function,

$$I(t) = I_1(0)e^{-t/\tau_1} + I_2(0)e^{-t/\tau_2} \quad (1)$$

where τ_1 and τ_2 are the slower and faster decay time constants, $I_1(0)$ and $I_2(0)$ represent the relative contributions of the slower decay and the faster decay components, respectively. Note that the biexponential decay process was often observed in $YVO_4:Eu^{3+}$ bulk powders or nanocrystalline powers. It is suggested that the slow decay components (τ_1) come from the transitions of Eu^{3+} ions locating at the perfect lattices, while the faster decay components (τ_2) originate from the emissions of Eu^{3+} ions near the defect states. For simplification, the decay time constants were averaged,

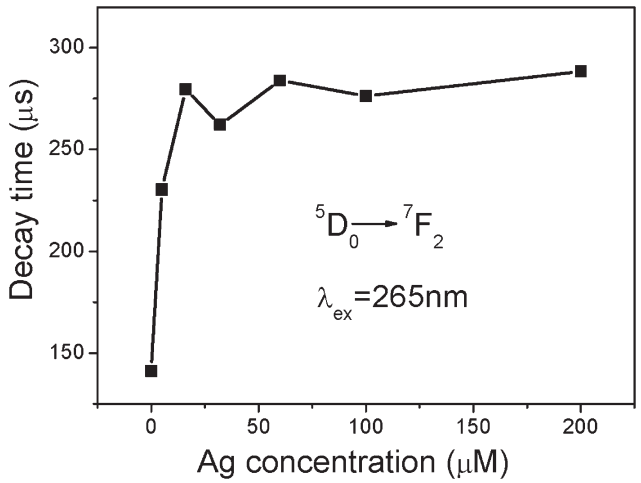

Fig. 6 Dependence of decay time constant of $^5D_0$–$^7F_2$ on the amount of silver nitrate (λ_{ex} = 265 nm) in YVO_4:Eu^{3+} NPs and YVO_4:Eu^{3+} @ Ag hybrids.

$$\tau = \frac{I_1(0)\tau_1^2 + I_2(0)\tau_2^2}{I_1(0)\tau_1 + I_2(0)\tau_2} \quad (2)$$

Fig. 6 shows the average decay time constants of $^5D_0$–$^7F_2$ transitions in a YVO_4:Eu^{3+}@Ag hybrid colloid sample as a function of the amount of silver nitrate, while the particle concentration in the solutions was fixed at 1 mg ml^{-1}. As can be seen, the average decay time constant of $^5D_0$–$^7F_2$ transition increases quickly and nearly doubles as the amount of silver nitrate increases in the range of 0–16 μM. As the amount of silver nitrate increases continuously, the average decay time constant of $^5D_0$–$^7F_2$ transitions changes little. There exist two possibilities for the improvement of decay time constants: (1) the decrease of radiative decay time constant and/or (2) the decrease of nonradiative time constant. Based on the considerable improvement of the $^5D_0$–^7F_J emission intensity, it is suggested that the nonradiative transition rate from $^5D_0$ decreases with the formation of silver NPs on YVO_4:Eu^{3+} NPs.

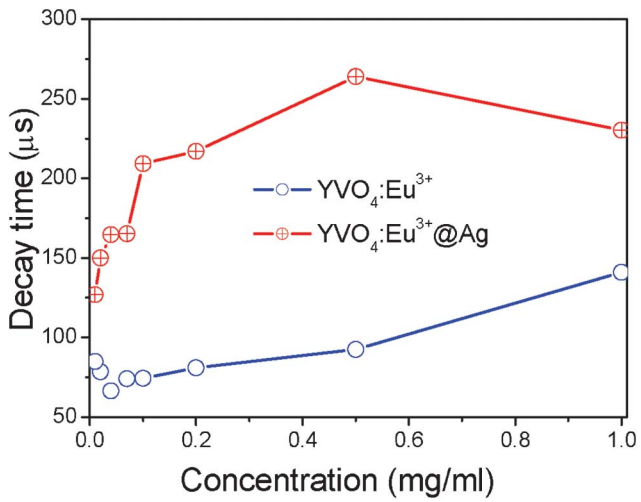

Fig. 7 Dependence of the decay time constant of $^5D_0$–$^7F_2$ on the particle concentration of YVO_4:Eu^{3+} NPs or YVO_4:Eu^{3+}@Ag hybrids in solution (λ_{ex} = 265 nm).

Actually, the particle concentration of YVO_4:Eu^{3+} or YVO_4:Eu^{3+}@Ag also has an obvious influence on the decay time constant of $^5D_0 \rightarrow {}^7F_2$ for Eu^{3+} ions. Fig. 7 shows the dependence of the decay time constants of the $^5D_0 \rightarrow {}^7F_2$ transition on the particle concentration of YVO_4:Eu^{3+} NPs or YVO_4:Eu^{3+}@Ag hybrids (5 μM silver nitrate). It is observed that as the particle concentration increases over a range of 0.01–1 mg ml^{-1}, where the decay time constant inYVO_4:Eu^{3+}@Ag gradually increases from 127 to 260 μs. In the YVO_4:Eu^{3+} NP colloids, the decay time constant has little variation when the concentration varies over 0.01–0.07 mg ml^{-1}. And as the concentration changes from 0.07–1 mg ml^{-1}, the decay time constant increases gradually from 74 to 141 μs. It is suggested that the increase of decay time constant with the increase of particle concentration is due to improvement of the reabsorption process. The reabsorption process represents the fraction of photons of the Eu^{3+} ions emission being absorbed once more, then remitted, reabsorbed, and so on. As a result, the decay time constant τ_1 is prolonged, which can be approximately described as:[26]

$$\tau_1 = \frac{\tau_0}{1 - \eta a} \quad (3)$$

where η and a represent the probability of photon re-emission and the reabsorption ratio respectively. And η should strongly depend on the spectral overlap between the emission of donors and the absorption of acceptors according to the Förster–Dexter theory, and be a constant with changing particle concentration. Because of the coefficient $\eta < 1$, this kind of reabsorption also induced the decrease in luminescence intensity, and because in solutions with dense NPs, aggregates of NPs were probably formed, leading to an increase in the optical path before the emitted light was scattered out of the solutions. As a consequence, a should increase with the increase in NP concentration. Because in the preparation of YVO_4:Eu^{3+} @Ag hybrids, sodium nitrate was added in the growth process and was insoluble in the ethanol, aggregates could form more easily. This may have lead to the reason why the luminescence intensity and decay time constant of the YVO_4:Eu^{3+} @Ag hybrids change more than the YVO_4:Eu^{3+} colloids with changing particle concentration.

The luminescent decay time constants of the $^5D_0 \rightarrow {}^7F_2$ transitions between the YVO_4:Eu^{3+} colloids and YVO_4:Eu^{3+}@ Ag hybrids in different solvents and powders were further compared, as shown in Table 1 It can be concluded that the decay time constants of YVO_4:Eu^{3+}@ Ag hybrid colloids become much longer than those in YVO_4:Eu^{3+} NPs. However, the decay time constants of YVO_4:Eu^{3+}@ Ag hybrids powders in air become a little bit shorter than those in YVO_4:Eu^{3+} NPs. In the powder samples, the nonradiative transition rates from $^5D_0$ to the down levels ^7F_J can be ignored due to very large energy gap of $^5D_0$–^7F_J ($\sim$11 200 cm^{-1}) and smaller phonon energy ($<$1000 cm^{-1}) of YVO_4 lattices according to the multi-phonon relaxation theory.[27] Therefore, the decay time constant of $^5D_0$–^7F_J transition is governed by the radiative transition rate. Because the radiative transition rate equals the inverse of the decay time constant, the radiative transition rate of $^5D_0$–^7F_J in YVO_4:Eu^{3+}@Ag hybrids increases a little in contrast to that in

$YVO_4:Eu^{3+}$ NPs. This may be due to the variation of effective refractive index (n_{eff}) in different samples. In nanocrystalline $YVO_4:Eu^{3+}$ powders, when the particle size is less than 1/4 wavelength of emission light, the effective refractive index can be written as, $n_{eff} \approx xn_{YVO_4^+}+(1-x)n_{air}$.[28] In $YVO_4:Eu^{3+}$@Ag hybrids, $n_{eff} \approx xn_{YVO_4^+}+(1-x)n_{Ag.}$ Because $n_{Ag} > n_{air,}$ the n_{eff} of $YVO_4:Eu^{3+}$@Ag should be bigger than that of $YVO_4:Eu^{3+}$. This will lead to the increase of radiative transition rate of $^5D_0$–^7F_J. Anyway, due to the low variation of the radiative transition rate, it can be concluded that the increase of the radiative decay rate of emitters is not the main reason for the luminescent enhancement.

D. The origin of luminescence enhancement behavior

Now let us carefully discuss the luminescent enhancement effect in $YVO_4:Eu^{3+}$@Ag hybrid colloids in comparison to the $YVO_4:Eu^{3+}$ NPs. According to the experimental results above, we consider that the main mechanism in this work for luminescent enhancement is neither the surface plasmon induced absorption enhancement of emitters due to the enhancement of the local electric field at the metal nanostructure surface, nor the increase of radiative decay rate of emitters due to the resonance of the emission with the surface plasmon of noble metals. The following facts are conflicted with the surface plasmon induced enhancement of the local electric field: (1) The absorption of VO_4^{3-} groups decreases with the increasing amount of silver NPs, instead of increasing; (2) The luminescence enhancement was observed only in $YVO_4:Eu^{3+}$@Ag colloids, but not in the powders; (3) In $YVO_4:Eu^{3+}$@Ag hybrid colloids, the decay time constants of $^5D_0$–$^7F_2$ increase greatly with the increased amount of silver NPs, but not in the powders, which should be independent of the enhancement of local electric field. The enhancement of the local electric field means an increase in incident light reaching the $YVO_4:Eu^{3+}$ NPs. We studied the dependence of the decay time constant of $^5D_0$–$\Sigma^7F_J(J = 2)$ on the power density of the excitation light, and the result indicated that as the density of excitation power increased ~one order, the decay time constant of $^5D_0$–$\Sigma^7F_J(J = 2)$ rarely changed for both the $YVO_4:Eu^{3+}$ NPs and the $YVO_4:Eu^{3+}$@Ag hybrids, implying that the enhancement of the local electric field can not induce the variation of decay time constant. The luminescent enhancement in the present case is also inverse to the increase of radiative decay rate of emitters due to the resonance of the emission with the surface plasmon of silver, as described above. In addition, the emission range of $^5D_0$–^7F_J for Eu^{3+} ions (550–700 nm) is far away from the surface plasmon absorption of silver NPs and the luminescent enhancement in $YVO_4:Eu^{3+}$@Ag hybrid colloids is nearly independent of emission wavelength, as can be seen in Fig. 4a.

Based on the above analysis, we believe that the main mechanism for the luminescent enhancement in $YVO_4:Eu^{3+}$@Ag hybrid colloids was induced by the interface effect in the solutions. To confirm this point, the quantum efficiency (QE) of $YVO_4:Eu^{3+}$@Ag hybrid colloids as a function of the silver nitrate amount was measured. The results demonstrated that the QE of pure $YVO_4:Eu^{3+}$ was only ~0.3%. The QE of $YVO_4:Eu^{3+}$@Ag hybrid colloids was improved to ~2.8% and nearly independent of the amount of silver nitrate as it varied from 5 μM to 100 μM. The QE increases about ~9.3 fold after coating, which is close to the luminescent enhancement factor (~9.8 fold). For the $YVO_4:Eu^{3+}$ and $YVO_4:Eu^{3+}$@ Ag nanopowders, the QE was determined to be ~11.8%. This indicates that in the solutions, the QE of $YVO_4:Eu^{3+}$ decreases more significantly than the corresponding nanosized powders due to the interaction between $YVO_4:Eu^{3+}$ nanophosphors and the solutions. The formation of Ag NPs on the surface of $YVO_4:Eu^{3+}$ can restrict the interaction of nanophosphors and the solutions. Generally speaking, in RE doped NPs the involvement of surface large vibration bonds such as OH^-, CO_3^{2-} will induce PL quenching due to the increase of nonradiative ET rate from hosts, RE ions to these bonds.[29] In the colloid solutions, the NPs should strongly interact with the solutions, such as ethanol, EG, DMF and H_2O. In other words, the energy on excited states of the host lattices and RE ions could be transferred to solutions through the interface interaction of the NPs with large vibration bonds of solutions as they are within the range of effective interaction length. It is suggested that in the $YVO_4:Eu^{3+}$@Ag hybrid colloids, the interaction of NPs with large vibration bonds of solutions was hindered, thus the luminescence intensity and the decay time constant of the $^5D_0$–^7F_J transition increased due to the decrease of the nonradiative transition rate. In order to reveal how the interaction of NPs with large vibration bonds of solutions was hindered in the $YVO_4:Eu^{3+}$@Ag hybrid colloids, the zeta potentials of the $YVO_4:Eu^{3+}$ colloids in the seed-mediated growth process (First Step) and the $YVO_4:Eu^{3+}$@Ag hybrids (Second Step) were investigated, as shown in Table 2. It can be seen that the zeta potential of the original $YVO_4:Eu^{3+}$ colloids solution is positive. After the formation of $YVO_4:Eu^{3+}$@Ag hybrids, the zeta potential of the solution becomes negative. This means that the surface of $YVO_4:Eu^{3+}$ is charge-positive, while the $YVO_4:Eu^{3+}$@Ag hybrids are charge-negative. It is suggested that in the former case, $YVO_4:Eu^{3+}$ can be bound effectively with OH^- bonds due to the charge gravitation between charge-positive NPs and charge-negative OH^- bonds, while in the latter case the charge-negative $YVO_4:Eu^{3+}$@Ag and OH^- bonds are repellant and can not be bound effectively each other. In the former case, ET from the surface of the $YVO_4:Eu^{3+}$NPs to OH^- bonds happens easily, leading to the quenching of PL. On the contrary, ET from the surface of the $YVO_4:Eu^{3+}$@Ag hybrids to OH^- bonds is suppressed, leading to luminescent enhancement. Fig. 8 gives the schematic illustration of the interface ET and PL processes of the $YVO_4:Eu^{3+}$ NPs and $YVO_4:Eu^{3+}$ @ Ag hybrids and the interaction mechanism for the $YVO_4:Eu^{3+}$ NPs and $YVO_4:Eu^{3+}$@Ag hybrids with ethanol solutions. In Fig. 8, when the VO_4^{3-} species are excited, the energy will be transferred to the Eu^{3+} ions and the hydroxyl in the solvent, respectively and part of the energy transferred to the Eu^{3+} ions will further transfer to the hydroxyl in the solvent from the $^5D_0$ level. Assuming that the radiative transition rate has little variation before and after silver coating, it is easy to deduce that

Table 2 Variation of the zeta potential and enhancement factor (En-factor) of the $YVO_4:Eu^{3+}$ colloids in the seed-mediated growth process and the $YVO_4:Eu^{3+}$@Ag colloids with changing the amount of silver nitrate

Ag^+(μM)	Y	Y+Ag^+	0	5	16	60	100
Zeta(mv)	0.85	0.89	−1.37	−2.37	−2.58	−2.11	−2.02
En-factor	1.0	1.4	2.0	9.8	8.9	7.5	5.3

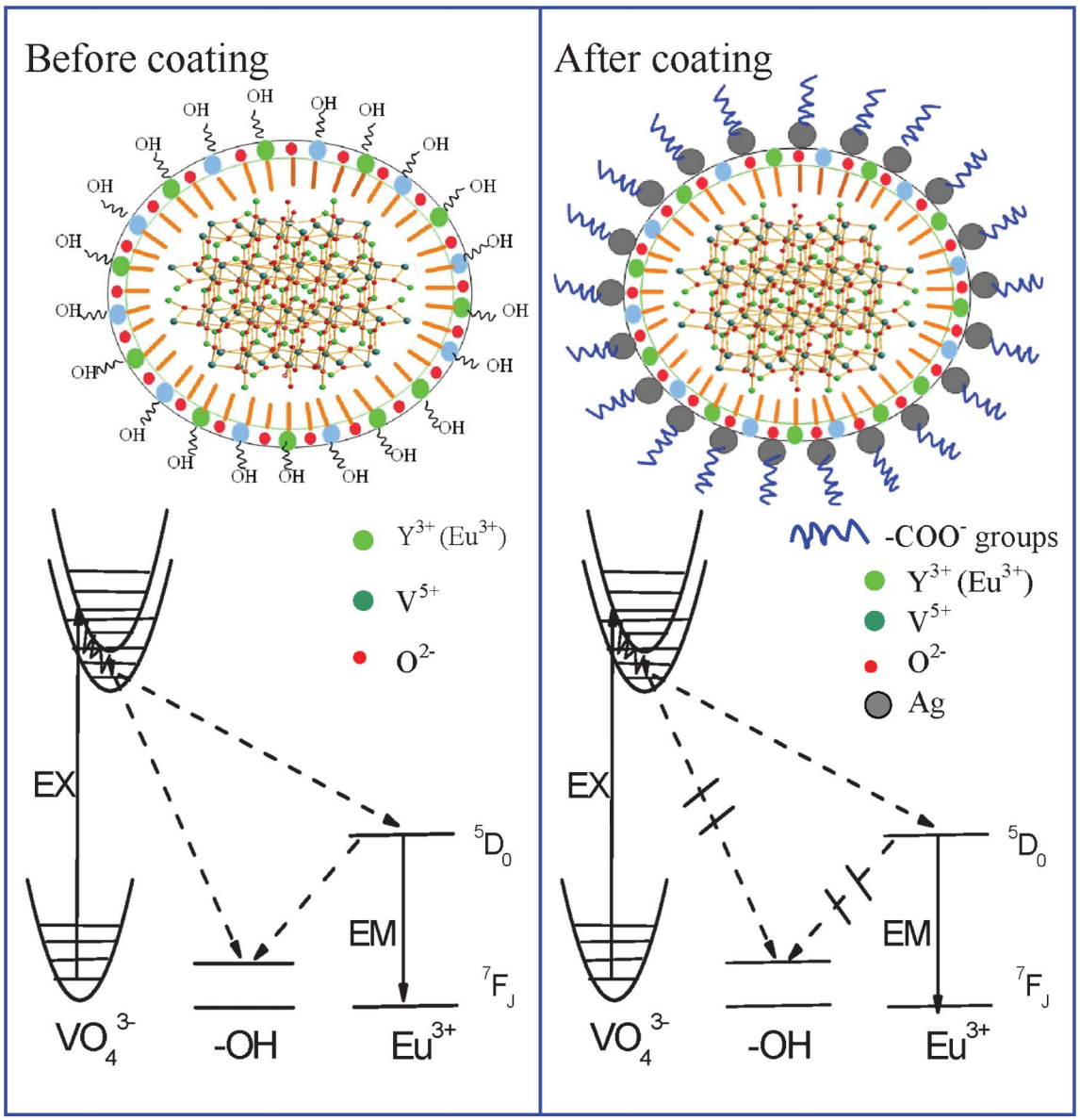

Fig. 8 Schematic illustration of ET and PL and luminescent enhancement processes of YVO_4:Eu^{3+} NPs and YVO_4:Eu^{3+}@ Ag hybrids.

the inner QE of Eu^{3+} on $^5D_0$ is inverse to the lifetime of $^5D_0$–^7F_J. Then it can be estimated that the inner QE of Eu^{3+} in the YVO_4 was improved ~2 times, while the ET efficiency from VO_4^{3-} species to Eu^{3+} ions was improved ~5 times in the optimum conditions of the dissolved solutions.

Finally, it should be further pointed out that such a highly luminescent enhancement was also observed on the YVO_4:Eu^{3+}@Au composites and the upconversion luminescence of YVO_4:Yb^{3+},Er^{3+} @Ag colloids. And more, most of nanophosphors should have strong and varied interactions with the solvents due to the complex preparation conditions of nanophosphor@noble metal composites, especially, the introducing of different surfactants. These will induce the change of the surface states of NPs and the interface interaction between NPs and solutions inevitably, leading to luminescent enhancement in different degrees. Therefore, we can claim that the present design for luminescent enhancement of YVO_4:Eu^{3+} will be of quite general nature for nanophosphor@noble metal composites in the solution phase.

IV. Conclusions

In this work, a facile seed-mediated growth of YVO_4:Eu^{3+}@Ag core-shell hybrid nanostructures colloids was realized. In the YVO_4:Eu^{3+}@Ag colloids, the luminescent enhancement of Eu^{3+} with a highest factor of ~one order of magnitude was observed when the amount of silver nitrate was 5 μM and the concentration of the YVO_4:Eu^{3+} colloids was 0.07 mg ml^{-1}. The enhancement factor decreased with further increase of the amount of silver NPs, which was caused by the scattering and reflection of silver NPs to excitation light. The luminescent decay dynamics was also systematically studied, and the results demonstrated that the decay lifetime constants of the $^5D_0$–$^7F_2$ transitions gradually increased with the increase of silver nitrate

and the increase in the $YVO_4:Eu^{3+}/YVO_4:Eu^{3+}$@Ag NP concentration. The luminescent mechanism was discussed based on various experiments, which indicated that the main mechanism for the luminescent enhancement in $YVO_4:Eu^{3+}$@Ag hybrids colloids originated from interface effect, rather than the surface plasmon induced absorption enhancement of emitters and/or the increase of radiative decay rate of emitters due to the resonance of the emission with the surface plasmon of silver NPs. In the $YVO_4:Eu^{3+}$@Ag hybrids, the nonradiative ET from the NPs to OH bonds of the solution was hindered considerably. A detailed model was proposed to explain the interesting luminescence enhancement behavior. This work is significant in obtaining efficient RE-doped hybrid colloids and aiding the understanding of the interaction of RE ions with noble NPs.

Acknowledgements

The authors would like to acknowledge National Talent Youth Science Foundation of China (Grant No.60925018),and the National Natural Science Foundation of China (Grant Nos. 20971051, 51002062, 11174111, and 61177042).

References

1 (*a*) A. J. Kenyon, *Prog. Quantum Electron.*, 2002, **26**, 225–284; (*b*) D. K. Matsuura, *Appl. Phys. Lett.*, 2002, **81**, 4526–4528.
2 (*a*) S. Q. Xu, H. P. Ma, D. W. Fang, Z. X. Zhang and Z. H. Jiang, *Mater. Lett.*, 2005, **59**, 3066–3068; (*b*) J. Zhang, S. W. Wang, T. J. Rong and L. D. Chen, *J. Am. Ceram. Soc.*, 2004, **87**, 1072–1075.
3 (*a*) M. Nyk, R. Kumar and Y. Tymish, *Nano Lett.*, 2008, **8**, 3834–3838; (*b*) H. Hu, M. G. Yu, F. Y. Li, Z. G. Chen, X. Gao, L. Q. Xiong and C. H. Huang, *Chem. Mater.*, 2008, **20**, 7003–7009; (*c*) Z. G. Chen, H. L. Chen, H. Hu, M. X. Yu and F. Y. Li, *J. Am. Chem. Soc.*, 2008, **130**, 3023–3029; (*d*) C. Louis, R. Bazzi and A. Christophe, *Chem. Mater.*, 2005, **17**, 1673–1682; (*e*) F. Zhang, R. C. Haushalter, R. W. Haushalter, Y. F. Shi, Y. C. Zhang and G. D. Stucky, *Small*, 2011, **7**, 1972–1976.
4 K. Kawano, B. C. Hong, K. Sakamoto, T. Tsuboi and H. J. Seo, *Opt. Mater.*, 2009, **31**, 1353–1356.
5 G. S. Y.i, H. C. Lu, S. Y. Zhao, Y. Ge, W. J. Yang, D. P. Chen and L. H. Guo, *Nano Lett.*, 2004, **4**, 2191–2196.
6 S. F. Lim, R. Riehn, W. S. Ryu, N. Khanarian, C. K. Tung, D. Tank and R. H. Austin, *Nano Lett.*, 2006, **6**, 169–174.
7 K. W. Krämer, D. Biner, G. Frei, H. U. Güdel, M. P. Hehlen and S. R. Lüthi, *Chem. Mater.*, 2004, **16**, 1244–1251.
8 J. Shen, L. D. Sun and C. H. Yan, *Dalton Trans.*, 2008, 5687–5697.
9 (*a*) D. Q. Chen, Y. L. Yu, Y. S. Wang, P. Huang and F. Y. Weng, *J. Phys. Chem. C*, 2009, **113**, 6406–6410; (*b*) M. B. Xie, Y. Tao, Y. Huang, H. B. Liang and Q. Su, *Inorg. Chem.*, 2010, **49**, 11317–11324.
10 (*a*) H. X. Mai, Y. W. Zhang, R. Si, Z. G. Yan, L. D. Sun, L. P. You and C. H. Yan, *J. Am. Chem. Soc.*, 2006, **128**, 6426–6436; (*b*) J. C. Boyer, F. Vetrone, L. A. Cuccia and J. A. Capobianco, *J. Am. Chem. Soc.*, 2006, **128**, 7444–7445.
11 (*a*) K. Riwotzki and M. J. Haase, *J. Phys. Chem. B*, 1998, **102**, 10129–10135.
12 (*a*) N. Liu, W. P. Qin, G. S. Qin, T. Jiang and D. Zhao, *Chem. Commun.*, 2011, **47**, 7671–7673; (*b*) W. Feng, L. D. Sun and C. H. Yan, *Chem. Commun.*, 2009, 4393–4395.
13 S. Eustis and M. A. El-Sayed, *Chem. Soc. Rev.*, 2006, **35**, 209–217.
14 W. L. Barnes, A. Dereux and T. W. Ebbesen, *Nature*, 2003, **424**, 824–830.
15 (*a*) T. Hayakawa, S. T. Selvan and M. Nogami, *J. Non-Cryst. Solids*, 1999, **259**, 16–22; (*b*) L. P. Naranjo, *Appl. Phys. Lett.*, 2005, **7**, 241914–241916; (*c*) T. Hayakawa, S. T. Selvan and M. Nogami, *Appl. Phys. Lett.*, 1999, **74**, 1513–151; (*d*) F. Zhang, G. B. Braun, Y. F. Shi, Y. C. Zhang, X. H. Sun, N. O. Reich, D. Y. Zhao and G. Stucky, *J. Am. Chem. Soc.*, 2010, **132**, 2850–2851; (*e*) X. N. Fang, H. W. Song, L. P. Xie, Q. Liu, H. Zhang and X. Bai, *J. Chem. Phys.*, 2009, **131**, 054506–054512; (*f*) L. Sudheen dra, V. Ortalan, S. Dey, N. D. Browning and I. M. Kennedy, *Chem. Mater.*, 2011, **23**, 2987–2993; (*g*) W. Deng, L. Sudhe en dra, J. B. Zhao1, J. X. Fu, D.Y. Jin, I. M. Kennedy and E. M. Goldys, *Nanotechnology*, 2011, **22**, 325604–3256011.
16 C. Louis, S. Roux, G. Ledoux, L. Lemelle, P. Gillet, O. Tillement and P. Perriat, *Adv. Mater.*, 2004, **16**, 2163–2166.
17 (*a*) J. Q. Gu, L. D. Sun, Z. G. Yan and C. H. Yan, *Chem.–Asian J.*, 2008, **3**, 1857–1864; (*b*) Z. Q. Li, L. M. Wang, Z. Y. Wang, X. H. Liu and Y. J. Xiong, *J. Phys. Chem. C*, 2011, **115**, 3291–3296; (*c*) M. Wang†, W. Hou†, C. C. Mi, W. X. Wang, Z. R. Xu, H. H. Teng, C. B. Mao and S. K. Xu, *Anal. Chem.*, 2009, **81**, 8783–8789; (*d*) J. Q. Gu, J. Shen, L. D. Sun and C. H. Yan, *J. Phys. Chem. C*, 2009, **112**, 6589–6593.
18 H. Zhang, Y. J. Li, I. A. Ivanov, Y. Q. Qu, Y. Huang and X. F. Duan, *Angew. Chem. Int. Ed.*, 2010, **49**, 2865–2868.
19 C. Hsu and R. C. Powell, *J. Lumin.*, 1975, **10**, 273–293.
20 J. H. Zhang, J. B. Liu, S. Z. Wang, P. Zhan, Z. L. Wang and N. B. Ming, *Adv. Funct. Mater.*, 2004, **14**, 1089–1094.
21 W. X.u, Y. Wang, X. Bai, B. Dong, Q. Liu, J. S. Chen and H. W. Song, *J. Phys. Chem. C*, 2010, **114**, 14018–14024.
22 L. Cheng, K. Yang, Y. G. Li, J. H. Chen, C. Wang, M. W. Shao, S. T. Lee and Z. Liu, *Angew. Chem., Int. Ed.*, 2011, **50**, 7385–7390.
23 L. P. Xie, H. W. Song, Y. Wang, W. Xu, X. Bai and B. Dong, *J. Phys. Chem. C*, 2010, **114**, 9975–9980.
24 K. Riwotzki and M. Haase, *J. Phys. Chem. B*, 2001, **105**, 12709–12713.
25 K. Riwotzki and M. Haase, *J. Phys. Chem. B*, 1998, **102**, 10129–10135.
26 W. Drozdowski and A. J. Wojtowicz, *Nucl. Instrum. Methods Phys. Res., Sect. A*, 2002, **486**, 412–416.
27 H. S. Peng, H. W. Song, B. J. Chen, J. W. Wang, S. Z. Lu, X. G. Kong and J. H. Zhang, *J. Chem. Phys.*, 2003, **118**, 3277–3282.
28 V. LeBihan, A. Pillonnet, D. Amans, G. Ledoux, O. R. Marty and C. Dujardin, *Phys. Rev. B*, 2008, **78**, 113405–113408.
29 G. Mialon, A. Alexandrou, T. Gacoin and J. P. Boilot, *J. Phys. Chem. C*, 2009, **113**, 18699–18706.

